



## Article

# Crystallography and Microstructure of 7M Martensite in Ni-Mn-Ga Thin Films Epitaxially Grown on (1 1 $\bar{2}$ 0)-Oriented Al<sub>2</sub>O<sub>3</sub> Substrate

Bo Yang <sup>1</sup>, Zongbin Li <sup>1</sup>, Haile Yan <sup>1</sup>, Yudong Zhang <sup>2,3</sup>, Claude Esling <sup>2,3</sup>, Xiang Zhao <sup>1</sup> and Liang Zuo <sup>1,\*</sup>

- <sup>1</sup> Key Laboratory for Anisotropy and Texture of Materials (Ministry of Education), School of Material Science and Engineering, Northeastern University, Shenyang 110819, China; yangb@atm.neu.edu.cn (B.Y.); lizb@atm.neu.edu.cn (Z.L.); yanhaile@atm.neu.edu.cn (H.Y.); zhaox@mail.neu.edu.cn (X.Z.)
- <sup>2</sup> Laboratoire d'Étude des Microstructures et de Mécanique des Matériaux (LEM3), CNRS UMR 7239, Université de Lorraine, CEDEX, 57045 Metz, France; yudong.zhang@univ-lorraine.fr (Y.Z.); claude.esling@univ-lorraine.fr (C.E.)
- <sup>3</sup> Laboratory of Excellence on Design of Alloy Metals for Low-mAss Structures (DAMAS), Université de Lorraine, CEDEX, 57045 Metz, France
- \* Correspondence: lzu@mail.neu.edu.cn

**Abstract:** Epitaxial Ni-Mn-Ga thin films have been extensively investigated, due to their potential applications in magnetic micro-electro-mechanical systems. It has been proposed that the martensitic phase in the  $\langle 1\ 1\ 0 \rangle_A$ -oriented film is much more stable than that in the  $\langle 1\ 0\ 0 \rangle_A$ -oriented film. Nevertheless, the magnetic properties, microstructural features, and crystal structures of martensite in such films have not been fully revealed. In this work, the  $\langle 1\ 1\ 0 \rangle_A$ -oriented Ni<sub>51.0</sub>Mn<sub>27.5</sub>Ga<sub>21.5</sub> films with different thicknesses were prepared by epitaxially growing on Al<sub>2</sub>O<sub>3</sub>(1 1  $\bar{2}$  0) substrate by magnetron sputtering. The characterization by X-ray diffraction technique and transmission electron microscopy revealed that all the Ni<sub>51.0</sub>Mn<sub>27.5</sub>Ga<sub>21.5</sub> films are of 7M martensite at the ambient temperature, with their Type-I and Type-II twinning interfaces nearly parallel to the substrate surface.

**Keywords:** Ni-Mn-Ga thin films; magnetically-induced reorientation; ferromagnetic shape memory alloys; crystallography



**Citation:** Yang, B.; Li, Z.; Yan, H.; Zhang, Y.; Esling, C.; Zhao, X.; Zuo, L. Crystallography and Microstructure of 7M Martensite in Ni-Mn-Ga Thin Films Epitaxially Grown on (1 1  $\bar{2}$  0)-Oriented Al<sub>2</sub>O<sub>3</sub> Substrate. *Materials* **2022**, *15*, 1916. <https://doi.org/10.3390/ma15051916>

Academic Editor: Rositsa Yakimova

Received: 31 December 2021

Accepted: 3 March 2022

Published: 4 March 2022

**Publisher's Note:** MDPI stays neutral with regard to jurisdictional claims in published maps and institutional affiliations.



**Copyright:** © 2022 by the authors. Licensee MDPI, Basel, Switzerland. This article is an open access article distributed under the terms and conditions of the Creative Commons Attribution (CC BY) license (<https://creativecommons.org/licenses/by/4.0/>).

## 1. Introduction

Ni-Mn-based ferromagnetic shape memory alloys have been considered as the promising materials for magnetic field-driven sensors and actuators, new type solid state refrigeration, and thermomagnetic generators [1–12]. Under the external magnetic-, thermal-, and force-field stimulus, they usually occur martensite variant reorientation and/or martensitic transformation [9–12], thus exhibiting multi-functionalities such as giant magnetic field-induced strain [1–5], excellent magnetocaloric effects [6–8], and colossal elastocaloric effects, etc. Among these functionalities, the giant magnetic field-induced strain has gained much attention, since both the single crystalline and polycrystalline bulk materials have demonstrated giant magnetic field-induced strain as much as 6–12% and 1% [1–5], respectively. Such giant magnetic field-induced strains also promote the research interest in epitaxial Ni-Mn-Ga thin films, as the films possess a cost-effective advantage in the application of magnetic micro-electro-mechanical systems [13–23]. So far, the magnetically induced reorientation of martensite variant has been reported in the  $\langle 1\ 0\ 0 \rangle_A$ -oriented Ni-Mn-Ga thin films epitaxially grown on the MgO(1 0 0) substrate and NaCl(1 0 0) substrate. Nevertheless, magnetic field-induced strains have not been achieved yet, since these kinds of thin films are of single crystalline state in the Austenite at evaluated temperatures and transform to self-accommodated martensite at ambient temperature. The self-accommodated martensite microstructure always contains two kinds of distinct microstructures: Type-X and Type-Y, which is composed of several different oriented martensite variants [17,24,25].

Recently, G. Jakob and his coworkers [26,27] proposed that the  $\langle 1\ 1\ 0 \rangle_A$ -oriented  $\text{Ni}_2\text{MnGa}$  thin films can be achieved by epitaxially growing on the  $(1\ 1\ \bar{2}\ 0)$  sapphire substrate ( $\text{Al}_2\text{O}_3$ ). In addition, the martensitic phase in the  $\langle 1\ 1\ 0 \rangle_A$ -oriented film on  $\text{Al}_2\text{O}_3$  substrate is much more stable than those in the  $\langle 1\ 0\ 0 \rangle_A$ -oriented film on  $\text{MgO}$   $(1\ 0\ 0)$  substrate. However, the martensitic transformation temperatures of the  $\langle 1\ 1\ 0 \rangle$ -oriented  $\text{Ni}_2\text{MnGa}$  thin films are between 260 K and 280 K, suggesting that the  $\text{Ni}_2\text{MnGa}$  thin films are of Austenite at ambient temperature. The magnetic properties, microstructure, and crystal structure of martensite in  $\langle 1\ 1\ 0 \rangle_A$ -oriented  $\text{Ni}_2\text{MnGa}$  thin films have not been revealed yet. A. Sharma and his coworkers [28] also prepared Ni-Mn-Ga thin films on  $(1\ 1\ \bar{2}\ 0)$  sapphire substrate ( $\text{Al}_2\text{O}_3$ ), which is of martensite at ambient temperature. However, the twinning interfaces of martensite are not parallel to the substrate surface [29], since the film thickness is of several micron meter.

In the present work, we successfully prepared the  $\langle 1\ 1\ 0 \rangle_A$ -oriented  $\text{Ni}_{51.0}\text{Mn}_{27.5}\text{Ga}_{21.5}$  films with different thicknesses from 200 nm to 600 nm on  $\text{Al}_2\text{O}_3$   $(1\ 1\ \bar{2}\ 0)$  substrates by magnetron sputtering. The characterization by X-ray diffraction technique, transmission electron microscopy revealed that all the  $\text{Ni}_{51.0}\text{Mn}_{27.5}\text{Ga}_{21.5}$  films are of 7M martensite at the ambient temperature, and with their Type-I and Type-II twinning interfaces nearly parallel to the substrate surface.

## 2. Materials and Methods

### 2.1. Thin Films Preparation

$\text{Ni}_{51.0}\text{Mn}_{27.5}\text{Ga}_{21.5}$  thin films with different thicknesses from 200 nm to 600 nm were grown on  $\text{Al}_2\text{O}_3$   $(1\ 1\ \bar{2}\ 0)$  mono-crystalline substrates by DC magnetron sputtering and using polycrystalline  $\text{Ni}_{48}\text{Mn}_{30}\text{Ga}_{22}$  as the target materials. The target is of 50.8 mm in diameter and 1.5 mm in thickness. Before deposition, the base pressure of the sputtering equipment was vacuumed to below  $9.0 \times 10^{-5}$  Pa. In order to obtain high-quality films, the substrate was heated to 650 °C. The sputtering process was conducted under a constant Ar working pressure of 0.15 Pa with an applied power of 70 W. Under this condition, the sputtering rate is of 0.1 nm/s roughly estimated through film thicknesses divided by deposition time. Before the actual depositions, a pre-sputtering was performed for 15 min.

### 2.2. Structure and Microstructure Characterization

The crystal structure and macroscopic crystallographic features were analyzed by temperature-dependent X-ray diffractometer using  $\text{Cu-K}\alpha$  radiation ( $\lambda = 0.15406$  nm) (Rigaku Smartlab 9 kW, Tokyo, Japan) and a four-circle X-ray diffractometer (Rigaku Smartlab 3 kW, Tokyo, Japan), respectively. A stylus profiler (Veeco DEKTAK 150, Plainview, NY, USA) was employed to measure the film thickness. The microstructures and chemical composition were examined by scanning electron microscopy (SEM, JEOL-JSM 7001F, Tokyo, Japan) and energy dispersive spectrometry (EDS, Bruker XFlash 4010, Berlin, Germany), respectively. The cross-sectional microstructures at nano and atomic scale were characterized by transmission electron microscopy (JEOL JEM 2100F, Tokyo, Japan) working at 200 kV. The cross-sectional sample for TEM characterization was prepared using the focused-ion beam (FIB, FEI Helios nanolab, Hillsboro, OR, USA) lift-out technique. Temperature-dependent magnetization curves and magnetic hysteresis loops were measured by Versalab (Quantum Design, San Diego, CA, USA).

## 3. Results and Discussion

### 3.1. Crystal Structure and Microstructure

Figure 1 displays the conventional and temperature-dependent X-ray diffraction patterns of the  $\text{Ni}_{51.0}\text{Mn}_{27.5}\text{Ga}_{21.5}$  thin films with different thicknesses from 200 nm to 600 nm grown on  $\text{Al}_2\text{O}_3$   $(1\ 1\ \bar{2}\ 0)$  mono-crystalline substrates. As shown in Figure 1a, it is seen that only one specific diffraction peak of  $\text{Ni}_{51.0}\text{Mn}_{27.5}\text{Ga}_{21.5}$  thin films is observed in the patterns, except the peaks from the  $\text{Al}_2\text{O}_3$  substrate, indicating that the films possess a strong preferred orientation. However, since the planar distance of  $(2\ 2\ 0)_A$  plane of

Austenite and  $(1\bar{2}\bar{1}0)_{7M}$  plane of 7M martensite are roughly equal, we cannot distinguish which specific diffraction peak belongs to the 7M martensite or the Austenite. We performed the temperature-dependent X-ray diffraction measurement, as shown in Figure 1b–d. As can be seen from Figure 1b–d, for all the films, with the increase in temperature, the specific diffraction peak of  $(1\bar{2}\bar{1}0)_{7M}$  gradually shifts to the low angle side. When the temperature is higher than 350 K, there is a sharp shift to the low angle side in the XRD patterns, which indicated that the  $(1\bar{2}\bar{1}0)_{7M}$  of 7M martensite transformed to the  $(2\ 2\ 0)_A$  of Austenite. It should be noted that the coexistence of Austenite and martensite phases in the 600 nm-thick  $\text{Ni}_{51.0}\text{Mn}_{27.5}\text{Ga}_{21.5}$  film, which may be due to the restriction from the substrate and the temperature is not high or low enough for the full martensitic transformation.

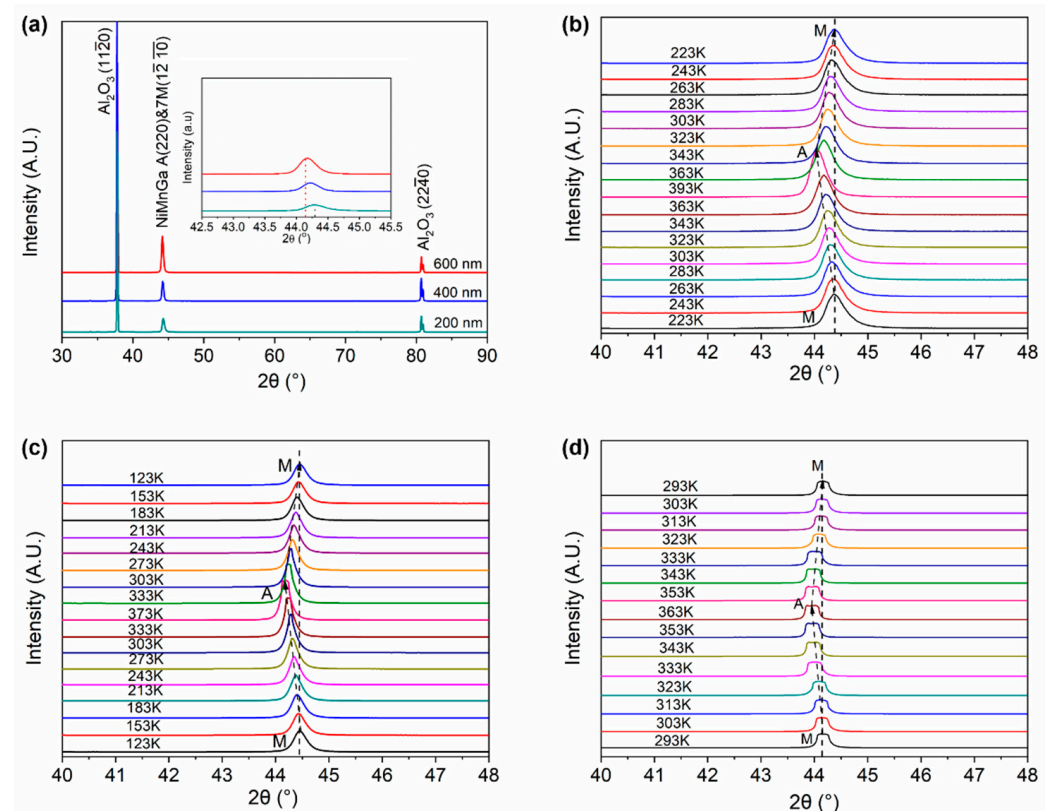


**Figure 1.** (a) X-ray diffraction pattern of  $\text{Ni}_{51.0}\text{Mn}_{27.5}\text{Ga}_{21.5}$  thin films with different thicknesses and (b–d) the corresponding temperature-dependent XRD patterns. (b) 200 nm, (c) 400 nm, and (d) 600 nm. In (b–d), A and M represent the Austenite and Martensite, respectively.

In order to determine the lattice parameters of the martensite, a four-circle X-ray diffractometer was employed to measure more XRD patterns at various azimuth angles ( $\Phi$ ) and tilt angles ( $\Psi$ ), as shown in Figure 2. With the employment of a four-circle XRD diffractometer, the crystal structure of the  $\text{Ni}_{51.0}\text{Mn}_{27.5}\text{Ga}_{21.5}$  thin films is identified as 7M modulated martensite and of monoclinic. The lattice parameters are shown in Table 1.

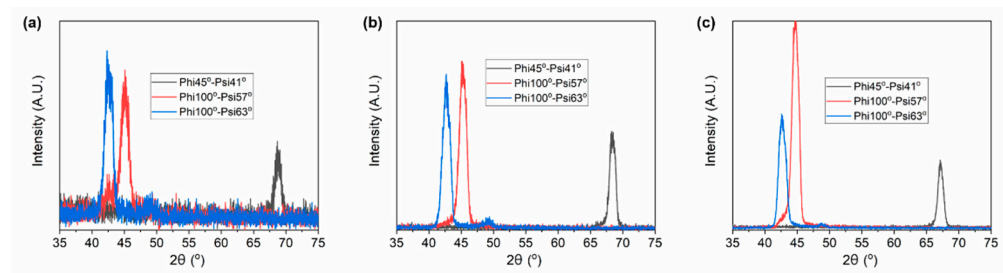
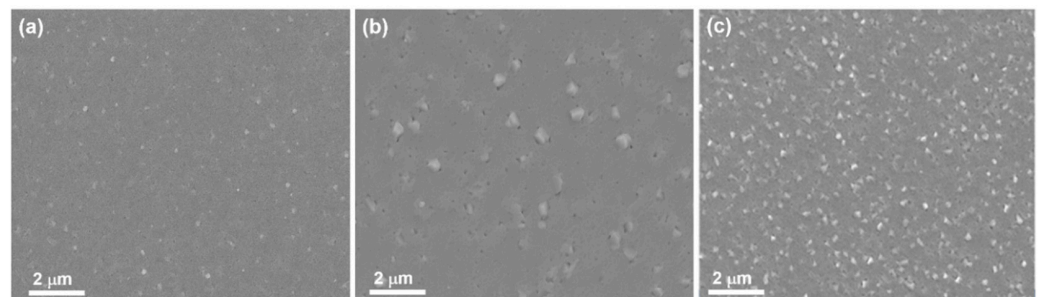


**Figure 2.** X-ray diffraction patterns of  $\text{Ni}_{51.0}\text{Mn}_{27.5}\text{Ga}_{21.5}$  thin films at various azimuth angles ( $\Phi$ ) and tilt angles ( $\Psi$ ). (a) 200 nm, (b) 400 nm, and (c) 600 nm.

**Table 1.** The lattice parameters of  $\text{Ni}_{51.0}\text{Mn}_{27.5}\text{Ga}_{21.5}$  thin films on  $\text{Al}_2\text{O}_3$  substrate.

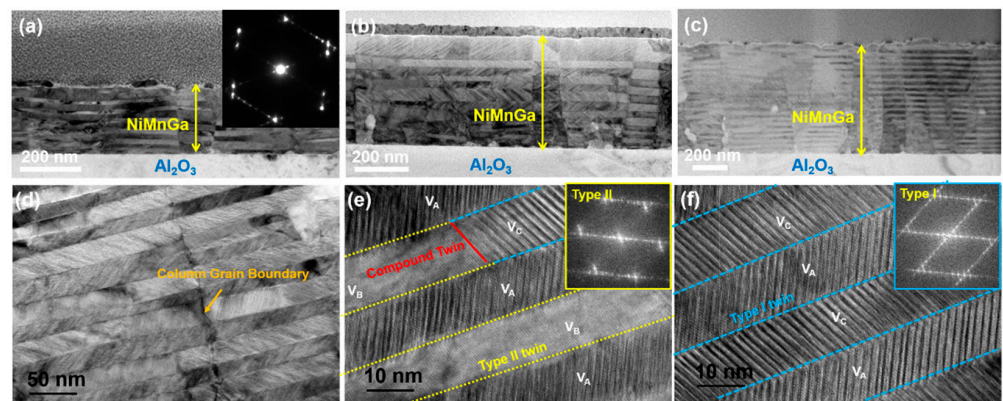
Thickness	Martensite	CS	a (Å)	b (Å)	c (Å)	$\beta$ (°)	V (Å <sup>3</sup> )
200 nm	7M	Monoclinic	4.188	5.446	42.46	93.12	966.9
400 nm	7M	Monoclinic	4.195	5.483	42.34	93.07	972.5
600 nm	7M	Monoclinic	4.164	5.566	42.63	93.03	986.7

Figure 3a–c shows the microstructure of  $\text{Ni}_{51.0}\text{Mn}_{27.5}\text{Ga}_{21.5}$  thin films with different thicknesses taken by FE-SEM. From these FE-SEM images, no twinning microstructure of the martensite variants can be observed in the top-view SEM images. All the films can be identified as continuously grown and the surface of the film becomes coarse with increasing thickness of the films. It is worth noting that white areas on the surface of the films can be identified as precipitates and the pit on the films might be defect pores among the column grains.



**Figure 3.** SEM images of  $\text{Ni}_{51.0}\text{Mn}_{27.5}\text{Ga}_{21.5}$  thin films. (a) 200 nm, (b) 400 nm, and (c) 600 nm.

To further analyze the microstructure and the martensitic configuration of the  $\text{Ni}_{51.0}\text{Mn}_{27.5}\text{Ga}_{21.5}$  films on the  $\text{Al}_2\text{O}_3$  substrate, the cross-section TEM characterization was conducted. As displayed in Figure 4a–c, the martensite is visible in all films. The twin interfaces of martensite are parallel to the substrate surface. A selected area electron diffraction confirmed that the martensite is of 7M martensite (insets in Figure 4a). In addition, with the increase in film thickness, the number of both martensite variants and the twin interfaces increased, but the thickness of each martensite variant remains unchanged. Even though the microstructure of all the films can be identified as column grains, a detailed observation in Figure 4d shows that the twin can pass the grain boundaries, which indicated that the column grain boundaries are small-angle grain boundaries. From Figure 4d–f, martensite can be classified as the hierarchical structure in which martensite lath incorporates martensitic variants. The further crystallographic analysis demonstrated that each plate corresponds to one crystallographic variant, there are a maximum of four-oriented variants in each group and Type-I twin, Type-II twin, and Compound twin are present in the film, which is marked as the dotted line.



**Figure 4.** Cross-sectional TEM bright-field images of  $\text{Ni}_{51.0}\text{Mn}_{27.5}\text{Ga}_{21.5}$  thin films. (a) 200 nm, (b) 400 nm, and (c) 600 nm. (d–f) Detailed analysis of the  $\text{Ni}_{51.0}\text{Mn}_{27.5}\text{Ga}_{21.5}$  thin films with a thickness of 600 nm.

### 3.2. Macroscopic Texture

In order to determine the orientation relationship between the variants and the substrate, X-ray diffraction was used to measure the pole figure of the  $\text{Ni}_{51.0}\text{Mn}_{27.5}\text{Ga}_{21.5}$  thin film with a thickness of 600 nm and the  $\text{Al}_2\text{O}_3$  ( $1\ 1\ \bar{2}\ 0$ ) substrate. As shown in Figure 5a,b, two symmetrically distributed spots appear at the  $\{0\ 0\ 0\ 1\}$  pole figures of the  $\text{Al}_2\text{O}_3$  substrate and three spots appear at the  $\{1\ 1\ \bar{2}\ 0\}$  pole figure of the  $\text{Al}_2\text{O}_3$  substrate. Thus, it can be determined that the edges of the substrate are parallel to  $\text{Al}_2\text{O}_3$   $[5\ \bar{5}\ 2]$  and  $\text{Al}_2\text{O}_3$   $[\bar{1}\ 1\ 1]$ . Thus, we choose  $\text{Al}_2\text{O}_3$   $[5\ \bar{5}\ 2]$ ,  $\text{Al}_2\text{O}_3$   $[\bar{1}\ 1\ 1]$  and  $\text{Al}_2\text{O}_3$   $[1\ 1\ 0]$  as the coordinate direction of the macroscopic sample coordinate system.

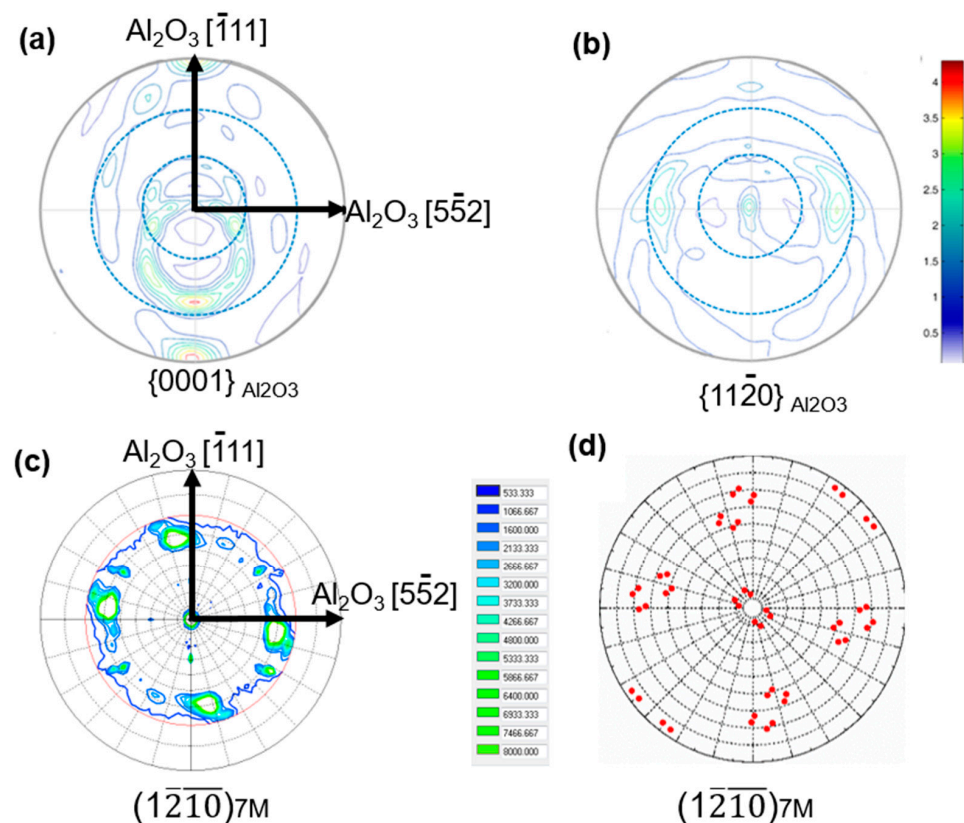


**Figure 5.** (a)  $\{0001\}_{\text{Al}_2\text{O}_3}$  and (b)  $\{11\bar{2}0\}_{\text{Al}_2\text{O}_3}$  pole figures of the  $\text{Al}_2\text{O}_3$  substrate, (c) measured and (d) theoretically calculated  $\{1\bar{2}\bar{1}0\}_{7\text{M}}$  pole figures of the  $\text{Ni}_{51.0}\text{Mn}_{27.5}\text{Ga}_{21.5}$  thin films with thicknesses of 600 nm.

As shown in Figure 5c, four spots appear at the  $\{1\bar{2}\bar{1}0\}_{7M}$  pole figures of the  $\text{Ni}_{51.0}\text{Mn}_{27.5}\text{Ga}_{21.5}$  thin film. The measured pole figure from the image of Figure 5c is in agreement with the theoretically predicted pole figure from the image of Figure 5d. Since the  $(1\bar{2}\bar{1}0)_{7M}$  plane of 7M martensite is parallel to the  $(2\ 2\ 0)_A$  plane of Austenite, we can conclude that the films were epitaxially grown on the  $\text{Al}_2\text{O}_3$   $(1\ 1\ \bar{2}\ 0)$  substrate, which justified that there is one crystallographic orientation for the Austenite in the present thin films. The crystallographic orientation of the Austenite can be described using Euler angle  $(60^\circ, 90^\circ, 45^\circ)$ . The mismatch relationship and the orientation of Austenite can also be determined, as shown in Figure 6. The  $\text{Al}_2\text{O}_3$   $[5\ \bar{5}\ 2]$  and  $\text{Al}_2\text{O}_3$   $[\bar{1}\ 1\ 1]$  direction parallel to the  $[1\ \bar{1}\ 1]_A$  and  $[1\ \bar{1}\ \bar{2}]_A$  direction of the Austenite of Ni-Mn-Ga thin films.

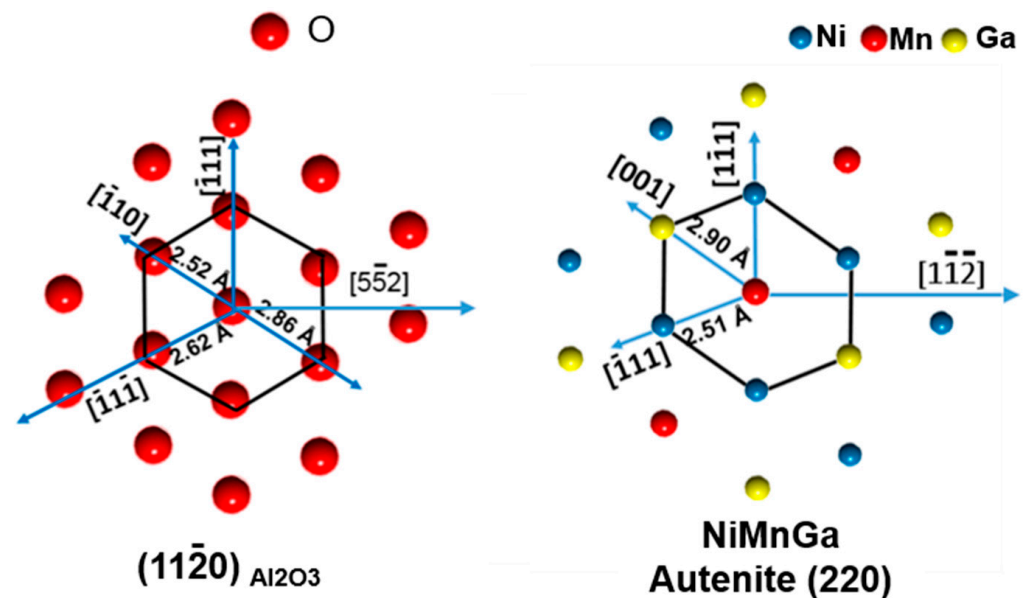


**Figure 6.** The mismatched relationship between the  $\text{Al}_2\text{O}_3$  substrate and the Austenite of Ni-Mn-Ga.

### 3.3. Magnetic Properties

Magnetization measurements are employed to identify the magnetic field-induced variant reorientation of the twin related martensitic variants in Ni-Mn-Ga thin films. Before the measurement of M-H loops, temperature-dependent magnetization curves were carried out to determine the martensitic transformation temperature as shown in Figure 7a. The M-T curves confirmed that the martensitic transformation temperature of the  $\text{Ni}_{51.0}\text{Mn}_{27.5}\text{Ga}_{21.5}$  thin films are above the ambient temperature, which suggested that these thin films are of martensite state at ambient temperature.

The magnetization hysteresis (M-H) loop of Ni-Mn-Ga thin films was measured at different temperatures, as shown in Figure 7b–d. “Magnetization jumps” in magnetization hysteresis loops can be a sign of the magnetic field-induced reorientation of martensitic variants. However, no obvious “magnetization jumps” can be found in magnetization hysteresis loops of the present  $\text{Ni}_{51.0}\text{Mn}_{27.5}\text{Ga}_{21.5}$  thin films with different thicknesses, from Figure 7b–d, which may be attributed to the high stress from the substrate.

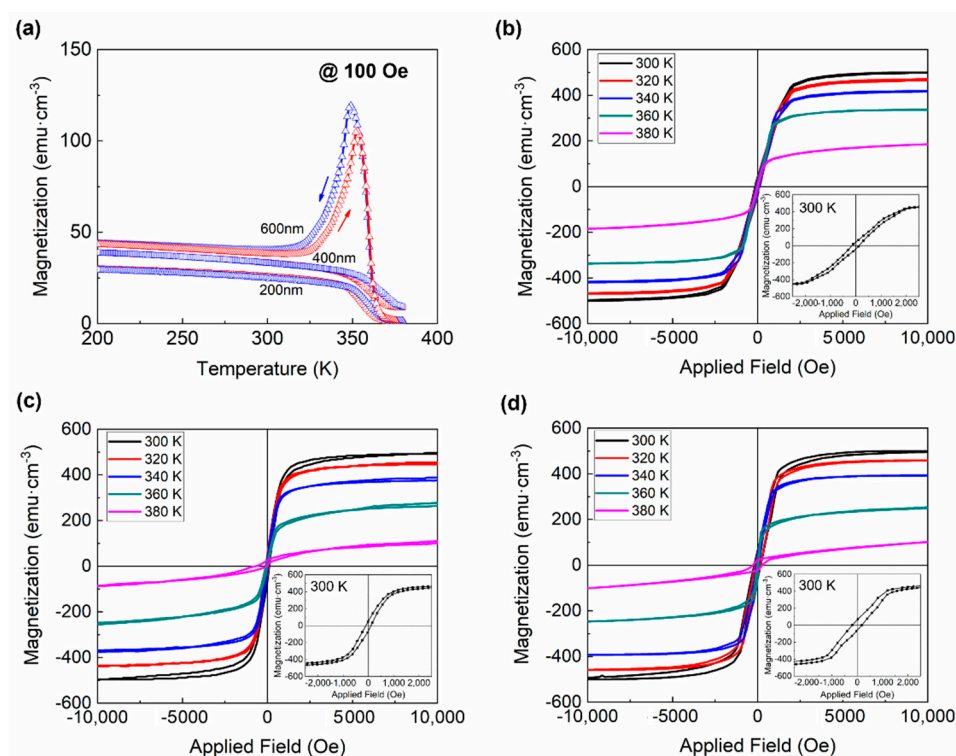


**Figure 7.** (a) Temperature-dependent magnetization cures and (b–d). Magnetization hysteresis loops at different temperatures of the  $\text{Ni}_{51.0}\text{Mn}_{27.5}\text{Ga}_{21.5}$  thin films. (b) 200 nm, (c) 400 nm, and (d) 600 nm.

#### 4. Conclusions

In summary, we deposited  $\langle 1\ 1\ 0 \rangle_A$ -oriented  $\text{Ni}_{51.0}\text{Mn}_{27.5}\text{Ga}_{21.5}$  thin films from 200 nm to 600 nm which are of monoclinic 7M at room temperature on the  $\text{Al}_2\text{O}_3$  (1 1  $\bar{2}$  0). X-ray diffraction and transmission electron microscopy characterization revealed that the martensite-related twin interfaces are parallel to the substrate, and each group possesses a maximum of four-oriented variants. Only one crystallographic orientation for the Austenite is in the thin film. The characterization of magnetic properties shows that the magnetic field-induced variant reorientation was not obvious in the present thin films.

**Author Contributions:** Conceptualization, B.Y.; validation, Z.L. and H.Y.; investigation, B.Y. and Y.Z.; writing—review and editing, C.E., X.Z. and L.Z.; supervision, C.E.; project administration, X.Z.; funding acquisition, L.Z. All authors have read and agreed to the published version of the manuscript.

**Funding:** This work was supported by the National Natural Science Foundation of China (Grant No. 52071071, 52171005), the Program of Introducing Talents of Discipline Innovation to Universities 2.0 (the 111 Project of China 2.0, No. BP0719037), the Fundamental Research Funds for the Central Universities of China (grant no. N2102006).

**Institutional Review Board Statement:** Not applicable.

**Informed Consent Statement:** Not applicable.

**Data Availability Statement:** The data presented in this study are available on request from the corresponding author.

**Conflicts of Interest:** The authors declare no conflict of interest.

#### References

- Murray, S.J.; Marioni, M.; Allen, S.M.; O’Handley, R.C.; Lograsso, T.A. 6% magnetic-field-induced strain by twin-boundary motion in ferromagnetic Ni-Mn-Ga. *Appl. Phys. Lett.* **2000**, *77*, 886–888. [[CrossRef](#)]
- Sozinov, A.; Likhachev, A.A.; Lanska, N.; Ullakko, K. Giant magnetic-field-induced strain in NiMnGa seven-layered martensitic phase. *Appl. Phys. Lett.* **2002**, *80*, 1746–1748. [[CrossRef](#)]

3. Sozinov, A.; Lanska, N.; Soroka, A.; Zou, W. 12% magnetic field-induced strain in Ni-Mn-Ga-based non-modulated martensite. *Appl. Phys. Lett.* **2013**, *102*, 021902. [[CrossRef](#)]
4. Gaitzsch, U.; Pötschke, M.; Roth, S.; Rellinghaus, B.; Schultz, L. A 1% magnetostrain in polycrystalline 5M Ni-Mn-Ga. *Acta Mater.* **2009**, *57*, 365–370. [[CrossRef](#)]
5. Li, Z.Z.; Li, Z.B.; Yang, B.; He, X.J.; Gan, W.M.; Zhang, Y.L.; Li, Z.; Zhang, Y.D.; Esling, C.; Zhao, X.; et al. Over 2% magnetic-field-induced strain in a polycrystalline Ni<sub>50</sub>Mn<sub>28.5</sub>Ga<sub>21.5</sub> alloy prepared by directional solidification. *Mater. Sci. Eng. A* **2020**, *780*, 139170. [[CrossRef](#)]
6. Guan, Z.; Jiang, X.; Gu, J.; Bai, J.; Liang, X.; Yan, H.; Zhang, Y.; Esling, C.; Zhao, X.; Zuo, L. Large magnetocaloric effect and excellent mechanical properties near room temperature in Ni-Co-Mn-Ti non-textured polycrystalline alloys. *Appl. Phys. Lett.* **2021**, *119*, 051904. [[CrossRef](#)]
7. Kuang, Y.F.; Ai, Z.R.; Yang, B.; Hao, X.W.; Li, Z.B.; Yan, H.L.; Zhang, Y.D.; Esling, C.; Zhao, X.; Zuo, L. Simultaneously achieved good mechanical properties and large magnetocaloric effect in spark plasma sintered Ni-Mn-In alloys. *Intermetallics* **2020**, *124*, 106868. [[CrossRef](#)]
8. Cong, D.Y.; Huang, L.; Hardy, V.; Bourgault, D.; Sun, X.M.; Nie, Z.H.; Wang, M.G.; Ren, Y.; Entel, P.; Wang, Y.D. Low-field-actuated giant magnetocaloric effect and excellent mechanical properties in a NiMn-based multiferroic alloy. *Acta Mater.* **2018**, *146*, 142–151. [[CrossRef](#)]
9. Zuo, L.; Li, Z.; Yan, H.; Yang, B.; Zhao, X. Texturation and Functional Behaviors of Polycrystalline Ni-Mn-X Phase Transformation Alloys. *Acta Metall. Sin.* **2021**, *57*, 1396–1415.
10. Liu, J.; Gottschall, T.; Skokov, K.P.; Moore, J.D.; Gutfleisch, O. Giant magnetocaloric effect driven by structural transitions. *Nat. Mater.* **2012**, *11*, 620–626. [[CrossRef](#)]
11. Kainuma, R.; Imano, Y.; Ito, W.; Sutou, Y.; Morito, H.; Okamoto, S.; Kitakami, O.; Oikawa, K.; Fujita, A.; Kanomata, T.; et al. Magnetic-field-induced shape recovery by reverse phase transformation. *Nature* **2006**, *439*, 957–960. [[CrossRef](#)] [[PubMed](#)]
12. Krenke, T.; Duman, E.; Acet, M.; Wassermann, E.F.; Moya, X.; Manosa, L.; Planes, A. Inverse magnetocaloric effect in ferromagnetic Ni-Mn-Sn alloys. *Nat. Mater.* **2005**, *4*, 450–454. [[CrossRef](#)] [[PubMed](#)]
13. Buschbeck, J.; Niemann, R.; Heczko, O.; Thomas, M.; Schultz, L.; Fähler, S. In situ studies of the martensitic transformation in epitaxial Ni-Mn-Ga films. *Acta Mater.* **2009**, *57*, 2516–2526. [[CrossRef](#)]
14. Eichhorn, T.; Hausmanns, R.; Jakob, G. Microstructure of freestanding single-crystalline Ni<sub>2</sub>MnGa thin films. *Acta Mater.* **2011**, *59*, 5067–5703. [[CrossRef](#)]
15. Ranzieri, P.; Fabbri, S.; Nasi, L.; Righi, L.; Casoli, F.; Chernenko, V.A.; Villa, E.; Albertini, F. Epitaxial Ni-Mn-Ga/MgO(100) thin films ranging in thickness from 10 to 100nm. *Acta Mater.* **2013**, *61*, 263–272. [[CrossRef](#)]
16. Backen, A.; Yeduru, S.R.; Diestel, A.; Schultz, L.; Kohl, M.; Fähler, S. Epitaxial Ni-Mn-Ga Films for Magnetic Shape Memory Alloy Microactuators. *Adv. Eng. Mater.* **2012**, *14*, 696–709. [[CrossRef](#)]
17. Ranzieri, P.; Campanini, M.; Fabbri, S.; Nasi, L.; Casoli, F.; Cabassi, R.; Buffagni, E.; Grillo, V.; Magen, C.; Celegato, F.; et al. Achieving Giant Magnetically Induced Reorientation of Martensitic Variants in Magnetic Shape-Memory Ni-Mn-Ga Films by Microstructure Engineering. *Adv. Mater.* **2015**, *27*, 4760–4766. [[CrossRef](#)]
18. Heczko, O.; Thomas, M.; Buschbeck, J.; Schultz, L.; Fähler, S. Epitaxial Ni-Mn-Ga films deposited on SrTiO<sub>3</sub> and evidence of magnetically induced reorientation of martensitic variants at room temperature. *Appl. Phys. Lett.* **2008**, *92*, 072502. [[CrossRef](#)]
19. Thomas, M.; Heczko, O.; Buschbeck, J.; Röbber, U.K.; McCord, J.; Scheerbaum, N.; Schultz, L.; Fähler, S. Magnetically induced reorientation of martensite variants in constrained epitaxial Ni-Mn-Ga films grown on MgO(001). *New J. Phys.* **2008**, *10*, 023040. [[CrossRef](#)]
20. Zhang, Y.P.; Hughes, R.A.; Britten, J.F.; Preston, J.S.; Botton, G.A.; Niewczas, M. Self-activated reversibility in the magnetically induced reorientation of martensitic variants in ferromagnetic Ni-Mn-Ga films. *Phys. Rev. B* **2010**, *81*, 054406. [[CrossRef](#)]
21. Yang, B.; Soldatov, I.; Chen, F.; Zhang, Y.; Li, Z.; Yan, H.; Schäfer, R.; Wang, D.; Esling, C.; Zhao, X.; et al. Observation of magnetic domain evolution in constrained epitaxial Ni-Mn-Ga thin films on MgO(001) substrate. *J. Mater. Sci. Technol.* **2022**, *102*, 56–65. [[CrossRef](#)]
22. Li, Z.B.; Yang, B.; Zou, N.F.; Zhang, Y.D.; Esling, C.; Gan, W.M.; Zhao, X.; Zuo, L. Crystallographic Characterization on Polycrystalline Ni-Mn-Ga Alloys with Strong Preferred Orientation. *Materials* **2017**, *10*, 463. [[CrossRef](#)]
23. Ghahfarokhi, M.T.; Casoli, F.; Fabbri, S.; Nasi, L.; Celegato, F.; Cabassi, R.; Trevisi, G.; Bertoni, G.; Calestani, D.; Tiberto, P.; et al. Martensite-enabled magnetic flexibility: The effects of post-growth treatments in magnetic-shape-memory Heusler thin films. *Acta Mater.* **2020**, *187*, 135–145. [[CrossRef](#)]
24. Yang, B.; Li, Z.B.; Zhang, Y.D.; Qin, G.W.; Esling, C.; Perroud, O.; Zhao, X.; Zuo, L. Microstructural features and orientation correlations of non-modulated martensite in Ni-Mn-Ga epitaxial thin films. *Acta Mater.* **2013**, *61*, 6809–6820. [[CrossRef](#)]
25. Yang, B.; Zhang, Y.D.; Li, Z.B.; Qin, G.W.; Zhao, X.; Esling, C.; Zuo, L. Insight into variant selection of seven-layer modulated martensite in Ni-Mn-Ga thin films grown on MgO(001) substrate. *Acta Mater.* **2015**, *93*, 205–217. [[CrossRef](#)]
26. Jakob, G.; Eichhorn, T.; Kallmayer, M.; Elmers, H.J. Correlation of electronic structure and martensitic transition in epitaxial Ni<sub>2</sub>MnGa films. *Phys. Rev. B* **2007**, *76*, 174407. [[CrossRef](#)]
27. Jakob, G.; Elmers, H.J. Epitaxial films of the magnetic shape memory material Ni<sub>2</sub>MnGa. *J. Magn. Magn. Mater.* **2007**, *310*, 2779–2781. [[CrossRef](#)]



- 
28. Sharma, A.; Mohan, S.; Suwas, S. Structural transformations in highly oriented seven modulated martensite Ni-Mn-Ga thin films on an Al<sub>2</sub>O<sub>3</sub> (11–20) substrate. *J. Mater. Res.* **2016**, *31*, 3016–3026. [[CrossRef](#)]
  29. Sharma, A.; Mohan, S.; Suwas, S. Evidence of adaptive modulation and magnetic field induced reorientation of variants in epitaxially grown Ni-Mn-Ga thin film on Al<sub>2</sub>O<sub>3</sub> (11–20) substrate. *Mater. Sci. Eng. B* **2019**, *242*, 6–16. [[CrossRef](#)]